Biol. Cybern. 71, 123–135 (1994)

Biological Cybernetics

Optimal control of antagonistic muscle stiffness during voluntary movements

Ning Lan, Patrick E. Crago

Applied Neural Control Laboratory, Department of Biomedical Engineering, Case Western Reserve University, Cleveland, OH 44106, USA

Received: 5 October 1991/Accepted in revised form: 18 November 1993

Abstract. This paper presents a study on the control of antagonist muscle stiffness during single-joint arm movements by optimal control theory with a minimal effort criterion. A hierarchical model is developed based on the physiology of the neuromuscular control system and the equilibrium point hypothesis. For point-to-point movements, the model provides predictions on (1) movement trajectory, (2) equilibrium trajectory, (3) muscle control inputs, and (4) antagonist muscle stiffness, as well as other variables. We compared these model predictions to the behavior observed in normal human subjects. The optimal movements capture the major invariant characteristics of voluntary movements, such as a sigmoidal movement trajectory with a bell-shaped velocity profile, an 'N'-shaped equilibrium trajectory, a triphasic burst pattern of muscle control inputs, and a dynamically modulated joint stiffness. The joint stiffness is found to increase in the middle of the movement as a consequence of the triphasic muscle activities. We have also investigated the effects of changes in model parameters on movement control. We found that the movement kinematics and muscle control inputs are strongly influenced by the upper bound of the descending excitation signal that activates motoneuron pools in the spinal cord. Furthermore, a class of movements with scaled velocity profiles can be achieved by tuning the amplitude and duration of this excitation signal. These model predictions agree with a wide body of experimental data obtained from normal human subjects. The results suggest that the control of fast arm movements involves explicit planning for both the equilibrium trajectory and joint stiffness, and that the minimal effort criterion best characterizes the objective of movement planning and control.

1 Introduction

A focus of motor control studies emphasizes the importance of the muscle spring-like property for movement execution (Rack and Westbury 1969; Nichols and Houk 1976; Hoffer and Andreassen 1981; Houk and Rymer 1981). This inherent compliance of the neuromuscular system unifies movement control and posture maintenance in a single scheme. Under steady state conditions, the joint can maintain a posture at the equilibrium point, at which the net joint torque is zero, but with a certain joint stiffness. A movement occurs as a result of changes in the equilibrium point of the system, because joint stiffness always causes a convergent force toward the equilibrium. It is postulated that the higher centers of the brain may guide joint movement by a gradual shift in equilibrium states, while maintaining a proper joint stiffness (Feldman 1986; Bizzi et al. 1992). This theory, known as the equilibrium point (EP) hypothesis, simplifies the task of motor control as it can obviate the need to calculate the inverse dynamics. In this study, we use optimal control theory as a forward dynamics approach to investigate (1) how the equilibrium trajectory is formulated, and (2) how the antagonistic muscles are controlled to produce the desired joint stiffness and the required joint torque for performing a movement.

According to EP control, a combination of equilibrium trajectory and joint stiffness must be specified to produce a movement. The choice for the form of control variables must be subject to constraints of neuromuscular dynamics and skeletal mechanics. For slow movements, it is possible to shift the equilibrium trajectory linearly in time towards the target position, while the joint stiffness is maintained constant throughout the movement (Feldman et al. 1990). However, for fast movements, experimental data obtained from normal human subjects indicate that the equilibrium trajectory and joint stiffness are not specified independently. The equilibrium trajectory appears to alternate about the movement trajectory with an 'N' shape, and there is a considerable amount of increase in joint stiffness during fast movements (Latash and Gottlieb 1991). Thus, the evidence suggests that both the equilibrium trajectory and joint stiffness are dynamically controlled to produce fast movements.

In earlier studies, a number of optimal criteria were proposed for movement planning and control. The minimal jerk criterion was used to describe the kinematics of

Present address and address for correspondence: Ning Lan, Ph.D., Wenner-Gren Research Laboratory, Center for Biomedical Engineering, University of Kentucky, Lexington, KY 40506, USA

movement trajectory, and it captured the details of the kinematics of voluntary movements (Hogan 1984). For the purpose of controlling a robot manipulator, it was proposed that the changes in the total joint torques may be minimized for controlling a movement (Uno et al. 1989). The trajectories of optimal joint torques and movement kinematics obtained with this criterion were found to be similar to those observed in human movements. Considering the psychophysical nature of movement planning, Hasan (1986) proposed that minimizing the effort associated only with the nonreflex drives of central descending commands may be a plausible criterion. In the context of EP control, these descending commands correspond to the equilibrium trajectory and an excitation signal that determines joint stiffness. Thus, Hasan (1986) formulated an effort functional as follows:

$$J = \int_0^{t_f} \sigma(t) * (\dot{\beta}(t))^2 \, dt \tag{1}$$

Here t_f is the duration of integration, $\dot{\beta}(t)$ is the time derivative of equilibrium trajectory, and $\sigma(t)$ is joint stiffness, which is time-varying in general. The optimal movements showed a normal looking trajectory with a bell-shaped velocity profile, and the optimal criterion also predicted the profile of the equilibrium trajectory with an alternating 'N' shape and a best constant joint stiffness for a movement.

In this study, we expand the scope of the model used in the optimization and investigate whether it is possible to determine both the equilibrium trajectory and joint stiffness simultaneously by minimizing the effort functional of (1). The optimization of the effort functional may lead to more meaningful results if a model at the muscular level is employed, and if the joint stiffness is not constrained to be a constant, since the optimization can then prescribe individual muscle stiffnesses and muscle activation inputs. Spinal reflexes are an integral part of the neuromuscular control system, and models that include descending commands to the motoneuron pools should also consider the effects of reflexes. The effects of autogenic reflexes are to enhance the stiffness of muscles in response to a stretch (Nichols and Houk 1976; Hoffer and Andreassen 1981). The effects of heterogenic reflexes on joint stiffness were demonstrated in recent experiments (Nichols and Koffler–Smuleviff 1991; Carter et al. 1993). Reciprocal inhibition between antagonist muscles can more effectively resist a perturbation at the joint. Feldman and Orlovsky (1972) further demonstrated that the shape of the length-tension property of muscles was maintained invariant by reflexes, and that only the threshold of this length-tension curve was affected by the stimulation of various supraspinal brain-stem structures.

The objective of this study is to develop and validate an optimal control model based on the EP hypothesis and the minimal effort criterion of (1). This model is then used to investigate whether a unique combination of the equilibrium trajectory and joint stiffness can be determined as a result of minimizing the effort functional for a given movement. Numerical solutions of the optimal control problem are obtained and compared with experimental data for model validation. The results obtained from this model can predict major features of voluntary movements observed in normal human subjects. In Sect. 2, the model structure is developed based on the physiology of neuromuscular control. The optimal control problem is formally formulated in Sect. 3, and the method used to obtain numerical solutions of the optimal control problem is briefly described. The results are analyzed in Sect. 4. In Sect. 5, the implications of the results are discussed in comparison with experimental data of voluntary movements.

2 Model development

2.1 General description

The hierarchical order of movement control is shown in Fig. 1. It is composed of an optimization algorithm, a spinal cord circuit that integrates descending and afferent signals, and a joint acted upon by a pair of antagonistic muscles. The higher center issues instructions to the control system, which specify the initial and

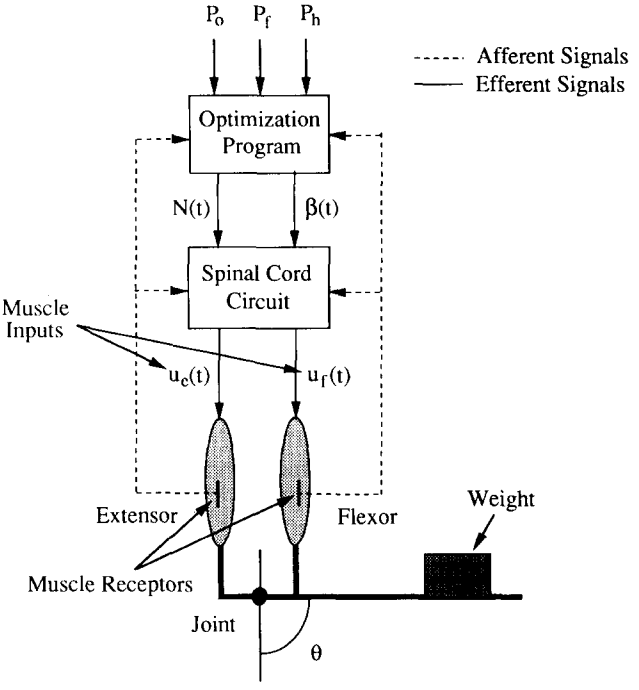

Fig. 1. The structure of the model. The control system comprises a pair of antagonistic muscles acting at a joint, a spinal cord integration circuit, and an optimization algorithm. The control inputs to the muscles, u_f and u_e, are the outputs of the spinal cord circuit that translates the descending motor commands into individual muscle activations. The descending commands to the spinal cord are the excitation signal, $N(t)$, and the equilibrium state, $\beta(t)$. The optimization program computes these descending commands based on the instructions from the higher center of the brain, which indicates the initial and final positions, P_0 and P_f, and the maximal level of the excitation, P_h. The joint is modeled as a hinge, and muscles have constant moment arms. The joint angle θ is defined such that it increases with flexion. The null angle corresponds to full extension of the joint

final joint positions (P_o, P_f) of movement and the maximal level of motoneuron pool excitation (P_h). These instructions are transformed into descending motor commands, encoding the equilibrium trajectory, $\beta(t)$, and the excitation signal, $N(t)$. The excitation signal activates the spinal motoneuron pools of muscles to the appropriate level. The outputs of the motoneuron pools are modified in accordance with peripheral events through autogenic and heterogenic reflexes, which are mediated by way of Ia afferents. Muscle proprioceptors (spindles and Golgi tendon organs) supply the spinal cord circuit and the optimal control algorithm with necessary peripheral information, such as muscle lengths, forces, and hence joint angles and torques. It is assumed that the effect of the autogenic reflexes is to regulate the muscle torque-angle relation, so that this torque-angle relation takes an invariant form. Thus, the autogenic reflexes can be accounted for by the muscle invariant property. The heterogenic reflexes act to modulate activities of the opposing muscle through reciprocal inhibition (RI) by way of the spinal interneurons. This coupling between antagonist muscles is explicitly considered in the model, because it reinforces EP control. The intensities of both reflexes are modulated by the background excitation of motoneuron pools (Gottlieb and Agarwal 1971; Matthews 1986). From a systems viewpoint, muscle torque-angle and torque-velocity properties can be equated as a nonlinear spring and a nonlinear damper. The mathematical model presented in the following section is based on this view of the neuromuscular motor system.

2.2 *Invariant characteristics of reflexive muscles*

Voluntarily contracting muscle with intact reflexes shows a linear relation between its stiffness and the torque (or force) it generates (Cannon and Zahalak 1982; Kearney and Hunter 1990; Carter et al. 1993). This linear relationship holds for a large range of muscle torque and stiffness, such that

$$T_f = m_f K_f + b_f; \quad T_e = m_e K_e + b_e \tag{2}$$

Here T_f and T_e are the torques, K_f and K_e are the stiffnesses, b_f and b_e are two constants, and m_f and m_e are constant coefficients. In the Appendix, it is shown that these relations, after integration with respect to the joint angle, define the exponential torque-angle invariant characteristics (ICs) for reflexive muscles, and that muscle activations change the threshold angle of the IC curves.

Muscle stiffness is assumed to be proportional to its activation $a_i(t)$:

$$K_i(t) = \kappa_i a_i(t) \quad 0 \leqslant a_i(t) \leqslant 1; \quad \text{for } i = \text{f, e} \tag{3}$$

Here κ_i is muscle stiffness at maximal activation. Subscript 'f' denotes the flexor muscle and subscript 'e', the extensor muscle. It is also shown in the Appendix that changes in muscle activation shift the muscle IC curve on the angle axis and consequently define a new equilibrium position.

Joint stiffness σ is the sum of individual muscle stiffnesses, and joint torque T is the net torque of antagonistic muscles as:

$$\sigma = K_f + K_e \quad \text{and} \quad T = T_f - T_e \tag{4}$$

2.3 *Muscle activation dynamics*

Since muscle stiffness is proportional to its activation [see (3)], we characterize muscle activation here as the ability to produce a torque (or force) under a unit stretch. A stretch at the joint affects the activations of the flexor and extensor muscles by both autogenic and heterogenic reflexes. In this model, the contribution of autogenic reflexes is accounted for by the muscle invariant curve (IC) of (2), and the effect of heterogenic reflexes is described later in Sect. 2.4.

A first-order differential equation describes the muscle activation dynamics as follows:

$$\frac{da_i(t)}{dt} = -\frac{1}{\tau_i} a_i(t) + \frac{1}{\tau_i} u_i(t) \quad 0 \leqslant u_i(t) \leqslant 1; \quad \text{for } i = \text{f, e} \tag{5}$$

Here $u_i(t)$ is the muscle neural input or the output of the corresponding motoneuron pool, $a_i(t)$ is the muscle activation, τ_i is the time constant for the muscle activation dynamics. The range of muscle input is confined between [0, 1]. With this constraint, muscle activation is also limited within the range [0, 1].

2.4 *Co-activation and reciprocal inhibition of antagonists*

Reciprocal activation and inhibition of antagonistic muscles are expressed as follows in this model:

$$u_f(t) = c(t)[0.5 + r_f(\beta(t) - \theta(t))] \tag{6a}$$

$$u_e(t) = c(t)[0.5 - r_e(\beta(t) - \theta(t))] \quad 0 \leqslant c(t) \leqslant 1 \tag{6b}$$

$$\frac{dc(t)}{dt} = -\frac{1}{\tau_N} c(t) + \frac{1}{\tau_N} N(t) \quad 0 \leqslant N(t) \leqslant 1 \tag{7}$$

Here $c(t)$ represents the background activation of the motoneuron pools for both flexor and extensor. This background activation is determined by the descending excitation signal, $N(t)$, as in (7). τ_N is the time constant of excitation; r_f and r_e are two positive constants for reciprocal inhibition gains.

Equations (6a) and (6b) emulate the physiological functions of spinal interneurons that mediate RI to the opposing muscle. The amplitude of inhibition is proportional to the difference between the equilibrium angle and the actual joint angle. If the joint angle coincides with the equilibrium angle, then there is no inhibition to the opposing muscle, but there could be a co-contraction if the background activation of the motoneuron pools is not zero, i.e. $c(t) \neq 0$. However, an angular perturbation at a joint will elicit different spindle responses for the flexor and extensor, because of their anatomical attachments around the joint. An increase in joint angle, $\theta(t)$, will cause the firing rates of flexor spindles to decrease because of shortening, but the firing rates of extensor spindles to increase because of lengthening. Thus, the

afferent from the two muscles varies in opposite sign with changes in the joint angle. The net effect of RI is to enhance joint stiffness to resist a perturbation (Nichols and Koffler–Smulevite 1991).

This spinal circuit can also facilitate the control of joint movement if the equilibrium angle, $\beta(t)$, is the variable. When the equilibrium angle is greater than the joint angle, a positive difference causes the flexor input, $u_f(t)$, to increase, while the extensor input, $u_e(t)$, is reduced. The net action is to move the joint towards the equilibrium angle. When the equilibrium angle is smaller than the joint angle, a negative difference suppresses flexor activation, but increases extensor activation. The net action is again to move the joint towards the equilibrium. Thus, RI guarantees a convergent force towards the equilibrium. In the limiting case, a large deviation of the equilibrium position from the joint position can completely suppress the opposing muscle and elicit a single muscle activation, as demonstrated in decerebrated cats (Nichols 1987). It is seen that co-contraction and reciprocal activation of antagonists are regulated by the descending excitation signal, $N(t)$, and the equilibrium trajectory, $\beta(t)$. There is also evidence that co-activation and reciprocal activation command centers exist in the brain of primates (Humphry and Reed 1983).

2.5 Limb dynamics

The dynamics of the forearm is of second order with a nonlinear viscosity. The arm is assumed as a rigid body with a rotational inertia. The joint is modeled as a hinge with a fixed center of rotation. Muscles are assumed to have constant moment arms. Joint dynamics are described by a second order nonlinear differential equation:

$$I\frac{d^2\theta}{dt^2}+B\frac{d\theta}{dt}=T \tag{8}$$

Here I is the moment of inertia, T is the net muscle torque, and B is the coefficient of viscosity. It was observed in human subjects that the viscosity changes with muscle stiffness (Cannon and Zahalak 1982; Lacquaniti et al. 1982; Kearney and Hunter 1990). However, different forms of relation between the coefficient of viscosity and muscle stiffness were suggested from the experimental data. Kearney and Hunter (1990) reported a square root relationship. Other data seemed to show a linear relationship (Cannon and Zahalak 1982). Both relations were found to yield movements with good agreement to experimentally observed trajectories (Flash 1987). In this study, a linear relation is used to simplify the model. The values of the model parameters used in the optimization are listed in Table 1.

2.6 Constraints

Constraints for this optimization problem are concerned with the range of joint movements, the activation threshold of the motoneuron pool, and the numerical range of neural signals. The range of movement is defined such that joint movement is possible. For the elbow joint, its work space may be limited to:

$$0^\circ \leqslant \theta(t) \leqslant 160^\circ \tag{9}$$

The physiological constraint considered here is the range of muscle stiffness that can be achieved. In this model, muscle stiffness is limited to being positive. Muscle inputs, thus, must also be positive, i.e. $u_i(t) \geqslant 0$ (i = f, e), as expressed in (6a) and (6b). However, this type of constraint is difficult to implement in numerical algorithms of optimization because of its discontinuous nature. However, an equivalent constraint of the form:

$$-\frac{1}{2r_f} \leqslant \beta(t)-\theta(t) \leqslant \frac{1}{2r_e} \tag{10}$$

can be easily implemented in the numerical algorithm. As a consequence, the equilibrium trajectory may saturate at the boundary to ensure the positiveness of muscle stiffness. Physiologically, when the equilibrium trajectory goes beyond the boundary, it produces no actual motoneuron pool output; thus, it is no longer valid. Within the boundary, the equilibrium trajectory obtained from the solution is the true optimization of the problem.

A final constraint considered here is the numerical range of the excitation signal, $N(t)$, which is limited within:

$$0 \leqslant N(t) \leqslant P_h; \quad \text{for } 0 < P_h \leqslant 1 \tag{11}$$

Here P_h denotes the maximal amplitude of the excitation signal. The physiological significance of the pulse height is that it limits the portion of the motoneuron pool which can be activated to perform a movement. These three constraints in (9), (10), and (11) together guarantee that the constraints in (3), (5), (6a), (6b), and (7) are satisfied, and they improve the numerical solvability of the optimal control problem.

3 Method of numerical solution

3.1 Problem formulation

A dynamic optimization problem has four parts that must be formulated (Kirk 1970; Bryson and Ho 1975). The essential part is the objective functional to be minimized. The second part is a mathematical description of the system, or a model. The complexity of the model

Table 1. Model parameters

Parameters	m_f (rad)	m_e (rad)	τ_f (ms)	τ_e (ms)	τ_N (ms)	κ_f (Nm/rad)	κ_e (Nm/rad)	I (kg·m^2)	B (Nm·s/rad)
Values	0.3	0.3	50	50	29	250	250	0.1	0.03σ

depends on whether the solution will yield meaningful interpretations. In our case, a model at the muscular level, as described in the previous section, is necessary. The third part of the problem is a set of constraints that define admissible solutions. The final part is a method to obtain the analytical, or numerical, solution.

To solve the optimal control problem, it is necessary to transform the above problem into the standard form of state-space representation. Reformulation of the problem is straightforward and can be done by properly defining state and input variables for the model. Let $\mathbf{x}(t)$ be the vector of states:

$$\mathbf{X}(t) = [\theta(t), \dot{\theta}(t), \beta(t), K_f(t), K_e(t), c(t)]^t$$

and $\mathbf{U}(t)$ be the vector of inputs:

$$\mathbf{U}(t) = [\dot{\beta}(t), N(t)]^t$$

The state-space equations for the system can then be expressed as:

$$\dot{\mathbf{X}} = \mathbf{f}(\mathbf{X}, \mathbf{U}) \tag{12}$$

Here $\mathbf{f}(\mathbf{X}, \mathbf{U})$ is a nonlinear vector function of states and inputs. The objective functional is rewritten in terms of states and inputs by:

$$J = \int_0^{t_f} g(\mathbf{X}, \mathbf{U}) dt \tag{13}$$

Here $g(\mathbf{X}, \mathbf{U})$ is the nonlinear cost function. The general form of constraints may be given by:

$$a_k \leqslant d_k(\mathbf{X}, \mathbf{U}) \leqslant b_k \quad \text{for } k = 1, 2, 3 \tag{14}$$

Here $d_k(\mathbf{X}, \mathbf{U})$ are the functions of states and inputs, respectively, and a_k and b_k are constants.

Let us define Ω as the set of all admissible controls within $[0, t_f]$, such that:

$$\Omega = \{\mathbf{U}(t) | a_k \leqslant d_k(\mathbf{X}, \mathbf{U}) \leqslant b_k; \text{ for } k = 1, 2, 3\}$$

The optimal control problem can then be stated as to find the optimal control policy $\mathbf{U}^*(t) \in \Omega$ for the system of (12) within $[0, t_f]$, such that it minimizes the cost functional of (13) and also satisfies the initial and final conditions:

$$\mathbf{X}(0) = \mathbf{X}_0 \quad \text{and} \quad \mathbf{X}(t_f) = \mathbf{X}_f \tag{15}$$

3.2 Nonlinear programming technique

A nonlinear programming (NP) algorithm, GAMS/MINOS (general algebraic modeling system and modular incore nonlinear optimization system; The Scientific Press, Redwood City, Calif.), is used to solve the dynamic optimization problem, since it permits constraints in the form of nonlinear equalities and inequalities as specified in (14). Before solving the dynamic optimization problem, it must be transformed into a static optimization problem, because the NP algorithm works only for static optimization. The numerical solutions were obtained on a CRAY supercomputer using the GAMS/MINOS software package.

The concept that GAMS/MINOS uses to solve dynamic optimization problems is briefly introduced below. The basic idea is to discretize the system (12), as well as the cost functional (13), and to linearize the system around an initial guess, $\mathbf{U}^k$. With this linearization, the cost functional and state variables are expressed as functions of inputs $\mathbf{U}$ and $\mathbf{U}^k$; the former is to be optimized, and the latter is taken from the previous kth iteration. The state equation of (12) can then be reduced to a set of nonlinear algebraic equations that enter into the NP problem as equality constraints. GAMS/MINOS solves the problem using a quadratically convergent algorithm (Robinson 1972). The search for a minimum is performed at two levels, the major iterations and minor iterations. In a major iteration, a number of linearly constrained subproblems are solved. Each subproblem constitutes a minor iteration. Minor iterations will stop if the subproblem is optimized. The solution is then returned to the major iteration. If the nonlinear constraints are satisfied, the major iteration stops, and an optimal solution is found.

In general, there is no guarantee that the algorithm will converge from an arbitrary starting guess. If it converges, the solution is likely to be a local minimum. However, in a region defined by the constraints and bounds of variables, if the objective functional and constraints are all convex, any optimal solution obtained will be a global minimum. In this problem, it is difficult to check the convexity of constraints because of its large dimension. However, the algorithm is always able to find a solution for a given movement.

3.3 Numerical analysis

The control of elbow movements at normal speeds is analyzed with this model. Model parameters used in the optimization are listed in Table 1. The flexor and extensor muscles are assumed to be symmetric and have the same biomechanical properties. The torque/stiffness ratios, m_f and m_e, are constants, having the same value of 0.3 (rad). The moment of inertia of the joint, I, is chosen to be 0.1 (kg m^2) in agreement with the literature (Hasan 1986). Joint viscosity is proportional to joint stiffness ($B = 0.03\sigma$). The maximal stiffnesses for the flexor and extensor muscles, κ_f and κ_e, are chosen to be 250 (Nm/rad) (Cannon and Zahalak 1982). Activation and excitation time constants are selected according to the literature (Winters and Stark 1987).

In the model, the initial and final positions and the maximal level of excitation (P_0, P_f and P_h) enter into optimization as externally applied constraints. For a movement specified by the initial and final positions, it is apparent that a different P_h may produce a different movement. Furthermore, a different gain for RI may alter the way the movement is performed. Sensitivity analysis is performed to investigate the effects of changes in model parameters on movement trajectories and muscle control inputs. Movements of very fast speed, about 0.2 (s) in duration, are solved first with the maximal level of excitation, i.e., with $P_h = 1$. Then the RI gains, r_f and r_e, are varied to show their effects on movement control.

We have also investigated how to produce a class of movements with different durations and distances by changing the upper bound of the excitation signal. In order to sort out the organizational base for behavioral regularities, different movements are normalized to a reference movement by scaling their velocity profiles in time and amplitude (Atkeson and Hollarbach 1985). Let us denote the amplitude of the reference movement as d_{ref} and its peak velocity as VP_{ref}. For an arbitrary movement with an amplitude denoted as d and a peak velocity as VP_{max}, normalization is performed according to the following rules:

$$V' = (VP_{ref}/VP_{max}) * V(t') \tag{16}$$

$$t' = (VP_{max}/VP_{ref}) * (d_{ref}/d) * t \tag{17}$$

Here V' and t' are the normalized velocity and time, respectively. In this normalization, the fastest movement with $P_h = 1$ is chosen as the reference movement. Behavioral regularities arising from the velocity scaling are further explored.

4 Results

Numerical solutions for single joint movements are presented and analyzed in this section. The general characteristics of optimal movements are described first in Sect. 4.1. The effects of RI gain and the amplitude of the excitation signal on the formation of movement trajectories and muscle control signals are investigated in Sects. 4.2 and 4.3, respectively. Section 4.4 demonstrates that movements with different amplitudes and durations can be achieved with a scaled velocity profile by properly modulating the excitation signal only.

4.1 Characteristics of optimal movements

A fast, point-to-point, optimal movement is presented in Fig. 2. The movement amplitude is 36° with a duration of about 0.2 (s). The speed is comparable to that of a ballistic movement by humans. Thus, the maximal amplitude of the excitation signal is used for this speed, i.e., $P_h = 1$. Joint movement and equilibrium trajectories are depicted in Fig. 2A. The joint movement shows a normal-looking sigmoidal trajectory, similar to that observed in voluntary movements. The equilibrium trajectory leads the movement trajectory initially to accelerate the joint, but then lags behind it to brake the movement. Overall, the equilibrium trajectory appears to show an 'N'-shaped profile. An overshoot of the equilibrium trajectory at the end of the movement establishes a steady-state terminal posture. This overshoot is less with slower movements. It is noted in Fig. 2A that the equilibrium trajectory has reached the boundary of constraint, as expressed in (10), during both acceleration and deceleration.

The velocity of joint movement (Fig. 2B) displays an asymmetrical, bell-shaped profile and is characterized by a shorter acceleration phase followed by a longer deceleration phase. The bell-shaped velocity is a well-

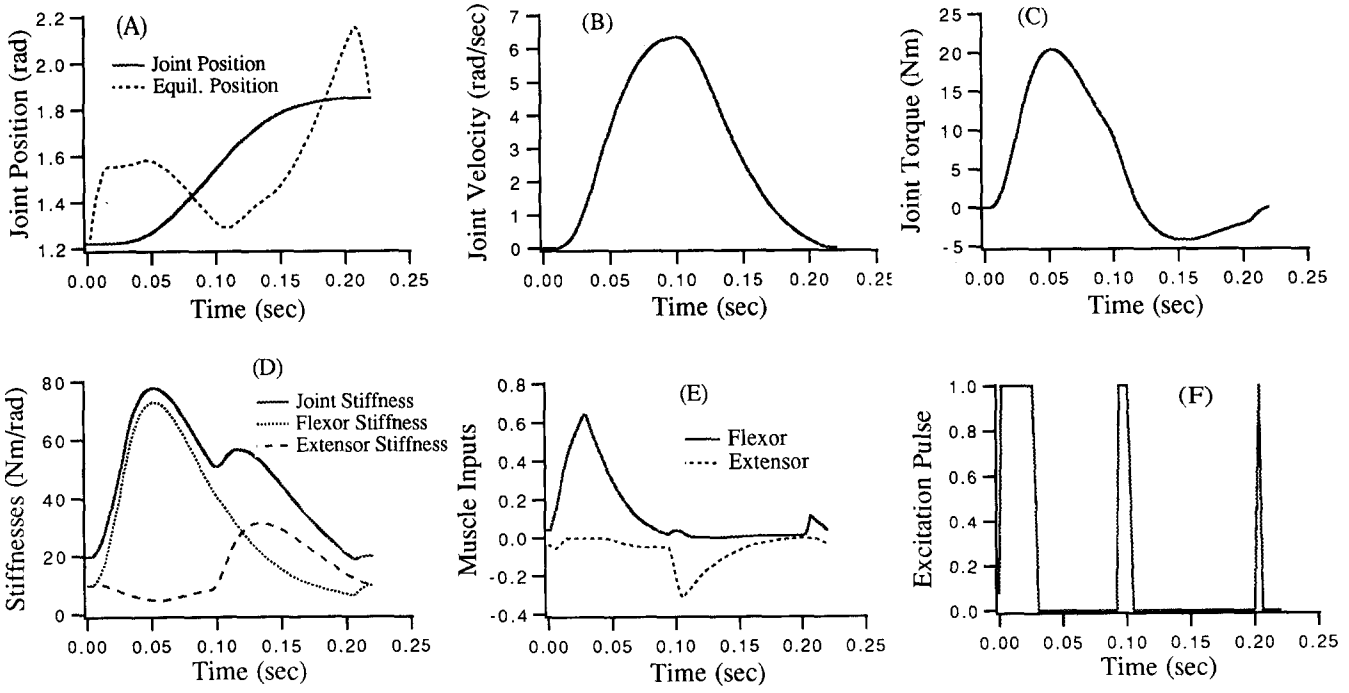

Fig. 2A–F. The optimal solution for a fast movement with a duration of about 220 ms. The movement amplitude is 36°. The maximal pulse height ($P_h = 1$) is used to generate the movement. **A** The movement trajectory, equilibrium trajectory; **B** joint velocity; **C** joint torque; **D** joint stiffness plus the flexor and extensor stiffnesses; **E** the muscle activation inputs; and **F** the excitation signal. Note that muscle inputs are all positive variables. The extensor activation is plotted with a negative sign to contrast with the flexor activation.

documented feature for single-joint arm or head movements (Nagasaki 1989). The torque responsible for accelerating the joint is much larger than that required to brake the joint (Fig. 2C). The imbalance in acceleration and deceleration efforts arises from the presence of joint viscosity, which is also a function of joint stiffness. Since viscous torque impedes movement acceleration but assists movement deceleration (Lestienne 1979; Wu et al. 1990), a greater flexor (agonist) input is often required to initiate the movement, and a smaller extensor (antagonist) input is necessary to stop the movement (Fig. 2E). Consequently, it leads to the asymmetric velocity profile.

Muscle activation inputs, u_f and u_e, are shown in Fig. 2E. They clearly display a triphasic burst pattern as in the EMG activities observed in voluntary movements. The first flexor burst is to accelerate the joint. The second burst of the extensor attempts to stop the joint motion. The third burst of the flexor establishes a steady-state joint stiffness for posture maintenance. An increase in joint stiffness occurs during the movement (Fig. 2D), which coincides with the rhythm of the triphasic muscle activation pattern. The optimal form of the excitation signal is a three-pulse signal (Fig. 2F), whose timing sets the rhythm of the triphasic muscle activities. The triphasic activation pattern and the three-pulse excitation signal are obtained with no prior assumption about their shape. These features are solely the prescription of the optimal criterion. Thus, it is significant that this model can predict the major features of voluntary movements.

4.2 Effects of reciprocal inhibition gain

RI plays an important part in translating the descending motor commands, $N(t)$ and $\beta(t)$, into muscle control inputs, $u_f(t)$ and $u_e(t)$. Simulations were performed with a range of RI gains from 0.5 to 5.0 for the fast movement (0.22 s and 36°) to see how RI gain changes affect movement control. The movements with various RI gains are presented in Fig. 3. It is found that the absolute value of RI gain has little effect on the movement kinematics and muscle controls, except for the equilibrium trajectory (Fig. 3A, B). As illustrated in Fig. 3D, E, and F, joint stiffness, muscle control signals, and excitation pulses are virtually unaffected by changes in the RI gain. For a smaller gain, a larger excursion in equilibrium trajectory is specified to compensate and the movements performed are virtually identical. When the difference between the equilibrium and movement trajectories is multiplied by the RI gain, it is found that this quantity is invariant (Fig. 3C). The value of the cost functional decreases with increased RI gain. This is attributed to the reduced excursion in equilibrium trajectory. These results show that movement control is insensitive to RI gain changes. Thus, the choice for the RI gain is irrelevant to the minimization of the cost functional. It could be specified to cope with other objectives of motor control.

4.3 Effects of excitation pulse height

The pulse height sets a limit on the extent to which the motoneuron pool can be maximally activated. To

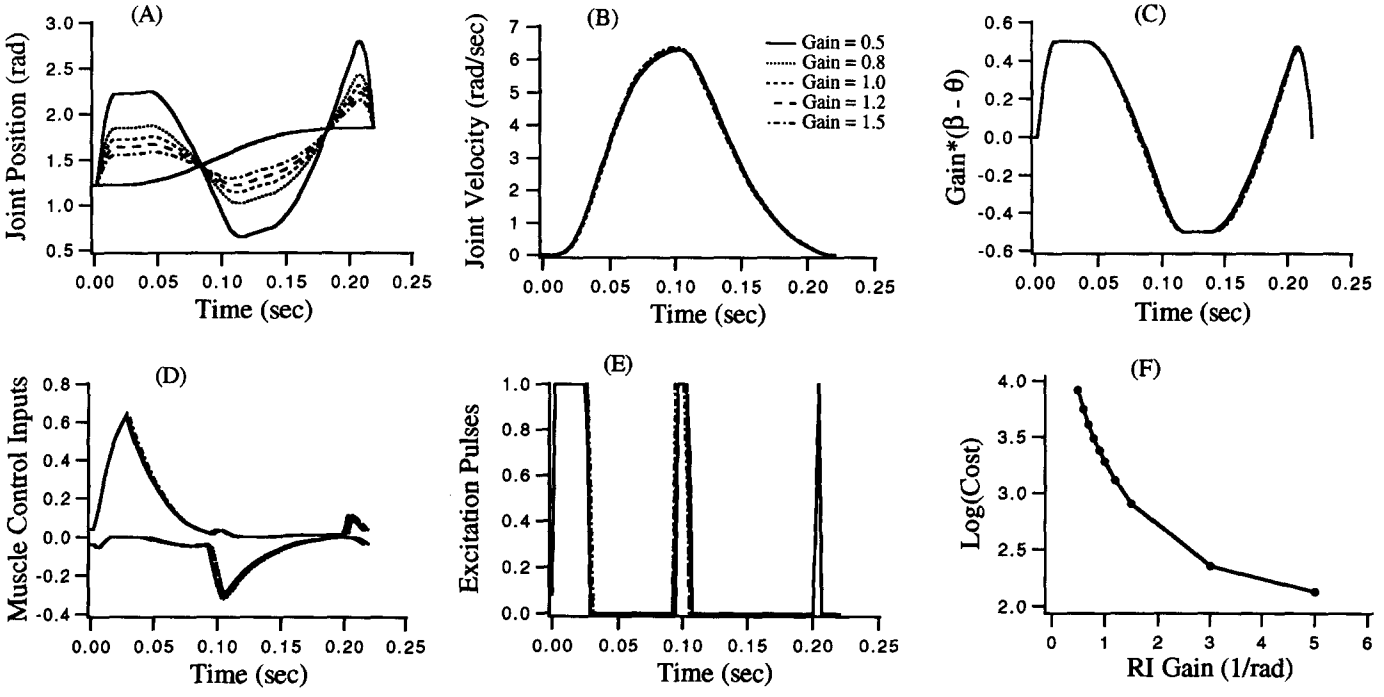

Fig. 3A–F. The effects of the reciprocal inhibition (RI) gain on the formation of movement trajectory and muscle controls. A 36° fast movement (220 ms in duration) is solved with a range of RI gains from 0.5 to 5.0. **A** The movement and equilibrium trajectories of different RI gains; **B** movement velocities; **C** the difference between the equilibrium and movement positions multiplied by the RI gain, which is invariant for all RI gains; **D** muscle activation inputs; **E** the excitation pulses; and **F** the relation between the values of the cost functional and RI grains

investigate the impact of this limit on movement control, sensitivity analysis is carried out with respect to changes in the pulse height. The movement used is of an amplitude of 36° and duration of 0.4 s. The height of the excitation pulse is varied from 1.0 to 0.2, and the numerical solutions are shown in Fig. 4.

It is apparent from Fig. 4 that the qualitative features of optimal movements are not altered by the pulse height. Muscle controls and velocity profiles still show the triphasic pattern and the bell-shaped appearance. Nevertheless, these movements show significant quantitative differences in movement trajectories, amplitude of muscle activation, and joint stiffness. In general, a greater pulse height tends to induce a quicker acceleration (Fig. 4B). Joint stiffness (Fig. 4C) and muscle activations (Fig. 4D) are elevated with increased pulse amplitude. A greater pulse height also elicits a higher level of co-contraction (Fig. 4D). The duration of excitation pulses is generally elongated when the pulse height is decreased (Fig. 4E). The cost decreases monotonically with the increased pulse height (Fig. 4F). While qualitative features of movement and control are preserved, quantitative details of kinematics and muscle activation are strongly affected by the height of the excitation pulse. This phenomenon may render the higher centers of the brain a simple and effective means for tuning motor behaviors. It further implies that the pulse amplitude could be chosen to serve other purposes, rather than minimizing the cost functional.

To compare the kinematic features of these movements with the fast movement, (16) and (17) are used to scale these movements with respect to the fast movement shown in Fig. 2. The normalized velocity profiles are presented in Fig. 5 together with the reference velocity. It is clear that the deceleration phase of all velocities line up very well with each other. The difference occurs mainly in the acceleration phase of movements. As the pulse height decreases, the rising edge of velocity rotates counterclockwise about that of the reference velocity. It is found that the velocity profile of a pulse height of 0.3 scales better with the reference velocity, among others. This indicates the existence of a movement whose velocity profile will superimpose best with that of the reference movement, and the pulse height of that movement should be in the neighborhood of 0.3. It appears that a congruent velocity profile may serve to normalize the otherwise widely different behaviors in movement kinematics and to simplify movement control.

4.4 Pulse height and duration modulation

The unique role of the excitation pulse in regulating the kinematic behavior offers the possibility to generate a class of movements with similar velocity profiles. Simulations were conducted to elucidate how the excitation pulse should be modulated to achieve similar velocity profiles. In the first set of simulations, movements of constant distance (36°) were performed with a range of durations from 0.22 to 0.5 (s). For each movement, the pulse amplitude is adjusted until the scaled velocity profile superimposes well with that of the reference. These movements are presented in Fig. 6. It is shown

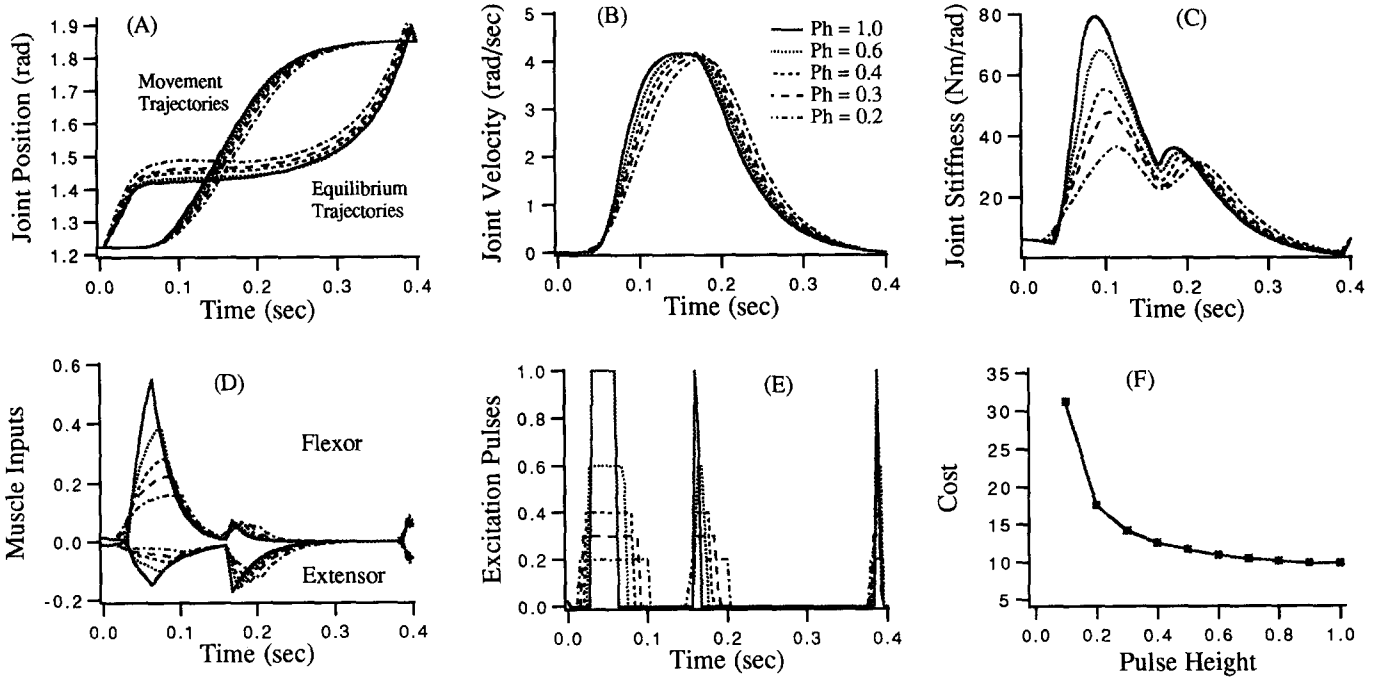

Fig. 4A–F. The effects of pulse height on the formation of movement trajectory and muscle controls. A slower movement of 400 ms in duration is solved with different P_h ranging from 1.0 to 0.2. The movement amplitude is 36°. **A** The equilibrium and movement trajectories obtained with different values of P_h; **B** the velocities; **C** the joint stiffnesses; **D** the muscle activation inputs; **E** the excitation signals; and **F** the relation between the value of the cost functional and the pulse height.

that all movement trajectories are similar to each other, except for the timing difference. The scaled velocity profiles superimpose well with the reference velocity. As the movement duration increases, the joint stiffness decreases as expected. The triphasic pattern of muscle control signals is preserved, but the magnitude of muscle activation decreases monotonically with the pulse height. The pulse duration is generally elongated for a smaller pulse height. It is shown that scaled movements with different durations can be achieved by pulse height modulation.

Another set of simulations was conducted to produce scaled movements of different distances by keeping the pulse height at 0.3 while adjusting the duration of the movement, which is equivalent to modulating the pulse duration. In these simulations, the movement distance ranges from 24° up to72°. For each amplitude, the movement duration is adjusted until the scaled velocity profiles superimpose well with the reference velocity. These movements are shown in Fig. 7. Clearly, all movements are indeed well scaled and have the same rate of initial acceleration, which is due to the fixed amplitude of the excitation pulse. For movements of a larger distance, the movement duration is generally increased, and so is the duration of the excitation pulses (Fig. 7F). The joint stiffness and magnitude of muscle activation are slightly different to make a movement of greater distance. This shows that it is not necessary to use a greater pulse height for moving a larger distance. Thus, it is possible to generate movements of different distances and durations by modulating the amplitude and duration of the excitation pulse.

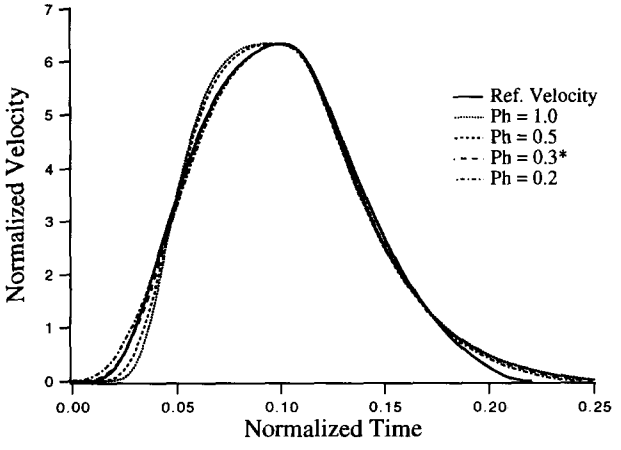

Fig. 5. Result after scaling the velocities of the movements in Fig. 4 with a reference movement. The reference movement is the fast movement presented in Fig. 2. The velocities are scaled both in time and in size. Only velocities of four pulse heights are shown along with the reference velocity. The velocity of a pulse height of 0.3 scales best with the reference movement among others.

5 Discussion

In this paper, we presented a model that is capable of predicting a wide variety of features of point-to-point,

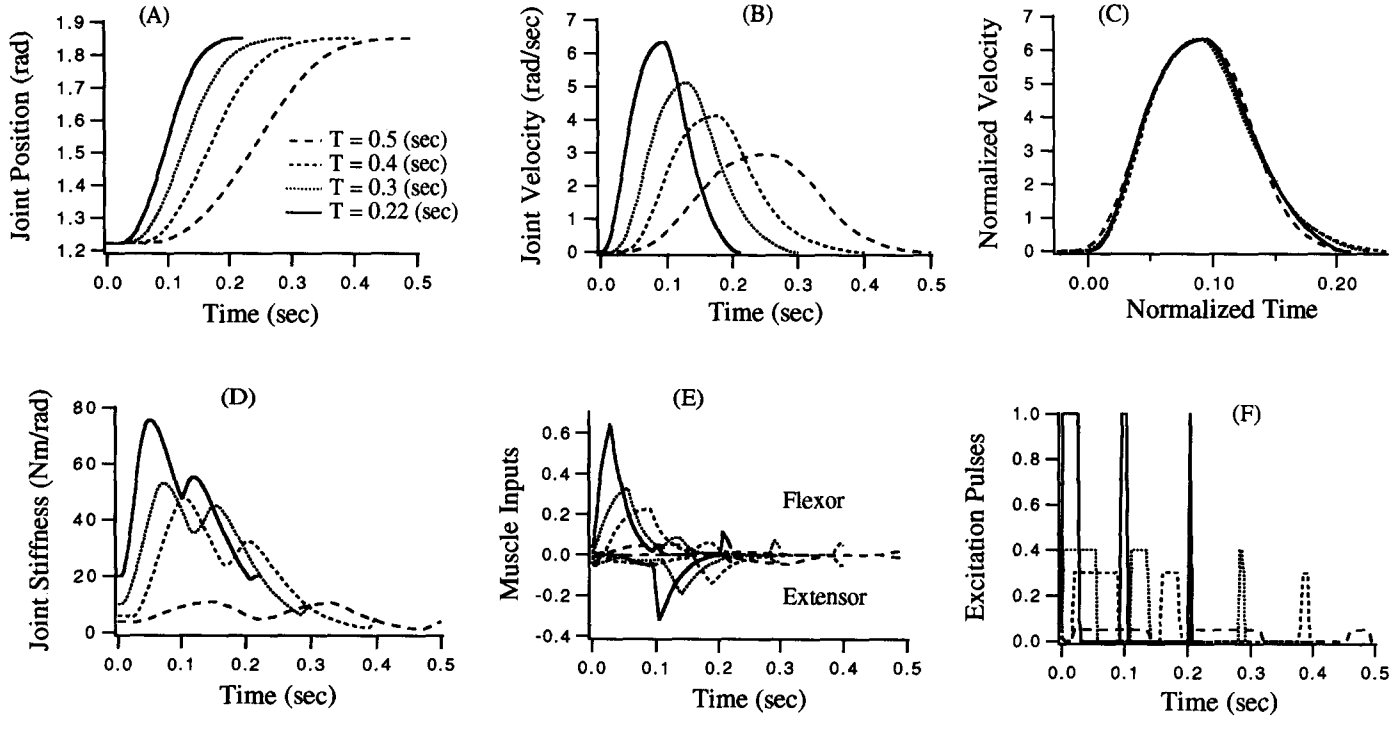

Fig. 6A–F. The movements with an amplitude of 36° and duration ranging from 200 to 500 ms. **A** Movement trajectories; **B** velocity profiles; **C** normalized velocities; **D** joint stiffness variations; **E** muscle activation inputs; and **F** excitation signals. For each movement, the pulse height is adjusted so that the resultant velocity profile is well scaled with that of the reference movement.

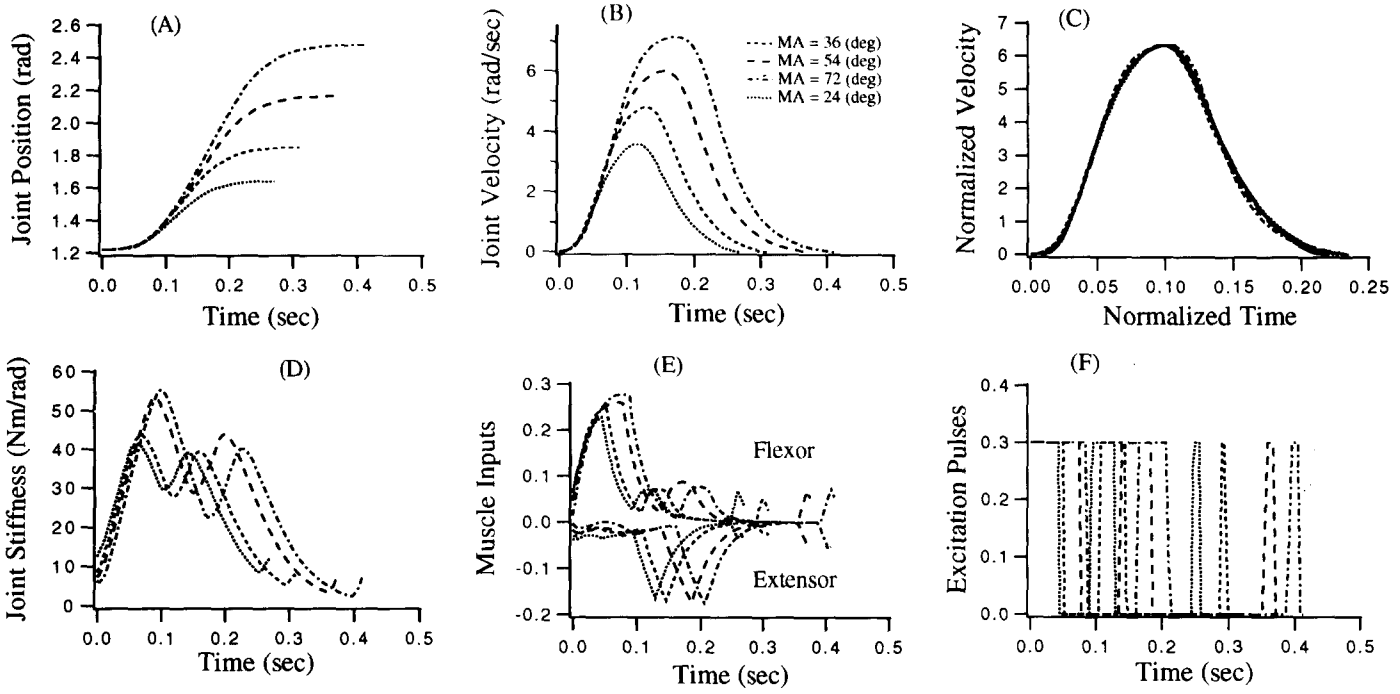

Fig. 7. The movements with amplitudes ranging from 26° to 72°. In this set of simulations, the pulse height is kept the same for all movements, but the movement duration is adjusted, so that the resultant velocity profile scales well with that of the reference movement. Adjusting the movement duration is equivalent to modulating the duration of the excitation pulses. **A** Movement trajectories; **B** joint velocities; **C** normalized velocities; **D** joint stiffness modulations; **E** muscle activation inputs; and **F** excitation pulses

single-joint arm movements, including (1) movement trajectory, (2) equilibrium trajectory, (3) muscle control inputs, and (4) muscle stiffness. The validity of the model predictions can be verified by comparing the qualitative features of optimal movements to published data from normal human subjects. However, caution must be taken when interpreting model predictions in comparison with experimental data. This is not to say that the actual neuromuscular control takes place in the exact way the model suggests. Instead, the comparison only implies that our model is able to replicate the qualitative behaviors of voluntary movements, and thus, the results make inference about the strategies that may be employed by the central nervous system (CNS) for movement planning and control.

The effort criterion of (1) used in this study penalizes unnecessarily high joint stiffness during movement and thus limits excessive co-contraction of antagonistic muscles. However, an intriguing result from our model is that the level of co-contraction is not solely determined by the optimal criterion, but is strongly affected by the pulse height as well. This is clearly shown in Fig. 4, in which the same movement is performed with different values of pulse amplitude, ranging from 0.2 to 1.0. The level of co-contraction increases with the pulse height, as does the joint stiffness accordingly. Thus, the joint stiffness is minimized only in the sense for a given maximal level of pulse height. The movements with a properly tuned pulse height are consistent with the observation that skilled voluntary movements in humans display little or no co-contraction in the antagonists (Gottlieb et al. 1989).

Sensitivity analysis shows that the pulse height is also the key parameter in regulating movement kinematics and joint stiffness. The choice of pulse height is independent of the optimal criterion but is dictated by the speed of movement. This independence lends the higher centers of motor control another degree of freedom to influence movement control. For example, the pulse height can be selected so as to generate a class of movements with scaled velocity profiles, as is shown in Fig. 6 and 7. The manner in which the amplitude and duration of the pulse height are modulated to generate the class of scaled movements is consistent with the dual strategy hypothesis (Gottlieb et al. 1989). Velocity scaling is a well-documented feature of voluntary movements in humans (Atkeson and Hollarbach 1985). This model, although simple, is able to distinguish the process of movement control from that of movement organization. The fact that an independent variable is required to normalize movement velocities indicates that movement scaling is not an inherent property of the minimal effort criterion.

Point-to-point arm movements carried out at normal speeds frequently display a triphasic activation pattern, where the agonist first fires strongly, followed by a slightly smaller burst in the antagonist, and ending with a small burst of activity in the agonist (Lestienne 1979; Marsden et al. 1983; Mustard and Lee 1987; Gottlieb et al. 1989; Karst and Hasan 1987). This pattern is clearly obtained in the muscle activation inputs of optimal movements (Fig. 2E). This feature remains unchanged for movements of different durations and amplitudes at normal speeds, as well as different pulse heights. This feature

corresponds to the three-pulse pattern in the excitation signal, $N(t)$. The model also duplicates the qualitative relation between EMGs and movement speeds observed under experimental conditions, which is characterized by monotonic functions of the EMG amplitude with respect to movement speed (Lestienne 1979; Marsden et al. 1983; Karst and Hasan 1987; Mustard and Lee 1987; Flanders and Herrmam 1992). A higher speed is always associated with an increased agonist activation. This monotonic relationship is clearly shown for movements of different durations (Fig. 6) and amplitudes (Fig. 7). Another noteable feature of optimal movements is the asymmetrical, bell-shaped velocity profile, which is a central characteristic of voluntary movements (Nagasaki 1989). This asymmetry arises from the presence of joint viscosity and may not be dominated by the optimal criterion. These regularities in motor behaviors reflect, in a large part, the necessity to move the joint in the most efficient way.

The model also predicts a dynamically modulated pattern of joint stiffness during movement, which increases during the movement and coincides with the rhythm of the triphasic muscle activations. In addition, the temporal variation of the EP during movement displays the 'N' shape. First, the EP leads the joint position. The difference between the EP and joint position provides acceleration of the joint. Then it lags behind the joint position to exert a braking torque at the joint. Finally, there is a small overshoot of the EP with respect to the final position, to restore the joint stiffness necessary to maintain the terminal posture. Such temporal variations of stiffness and equilibrium trajectory can be expected from the optimal criterion. This is apparent from (1), since a reciprocal variation between the joint stiffness and equilibrium trajectory is favorable for minimizing the effort functional. Thus, when a large variation in the equilibrium trajectory occurs, such as at the beginning and end of the movement, the joint stiffness is low. However, when the change in the equilibrium trajectory is small, such as in the middle of the movement, the joint stiffness increases rapidly. Consequently, this leads to the 'N' shape of the equilibrium trjectory. This shape is also necessary to alternate the activations of the antagonist muscles for acceleration and braking.

These outcomes of optimization are in agreement with available experimental measurements in subject-initiated elbow movements. In an attempt to reconstruct equilibrium trajectory and joint stiffness, Latash and Gottlieb (1991) designed an experiment in which subjects were asked to move their elbow joint against a bias load with a 'do-not-intervene' instruction. An EP control model was used to recover the equilibrium trajectory and joint compliance (the inverse of joint stiffness). For fast elbow movements, they found that the equilibrium trajectory led the joint angle initially but lagged behind the joint movement toward the end of the movement, showing a 'N'-shaped profile. Experimental results reveal a large phasic increase in joint stiffness in the middle of the movement. This empirical evidence substantiates our model predictions. In quick point-to-point movements in the horizontal plane, the initial and final stiffnesses required to maintain static postures are small, while the stiffness required to accelerate and decelerate the joint may be much higher. Therefore, an increase in joint stiffness is expected to occur during the movement. However, in slow and cyclic movements, the pattern of joint stiffness variation and the shape of the equilibrium trajectory may be different (Bennett et al. 1991; Latash 1992).

The CNS may use a motor program to compute the descending excitation signal, $N(t)$, and the equilibrium trajectory, $\beta(t)$. The inputs to the motor program are the initial and final positions and the pulse height; the latter is related to the speed of the movement. In essence, the motor program maps the target position into a trajectory of the EP that is associated with a temporal pattern of joint stiffness. The temporal variation of the joint stiffness is determined by the equilibrium trajectory and the excitation signal. These two descending commands are further translated into neural control inputs to individual muscles by a spinal neural network, where the RI plays an important role for this transformation. Equations (6a) and (6b) indicate that the mechanism of RI guarantees a convergent force towards the equilibrium. RI also enhances the efficacy of movement control, because it tends to reduce the co-activation of antagonists during movement. If RI were not present, an equilibrium trajectory could still be specified by the motor program, but the movement would be performed with a higher degree of co-contraction in the antagonists as (6a) and (6b) suggest. This is consistent with the observation that deafferentation in monkeys did not impair their ability to perform movements, but the movements were performed with a higher degree of co-contraction in the antagonists (Bizzi et al. 1978). This suggests that the overall structure of the model corresponds well to the neuromotor control system in vertebrates. The model is also useful as a motor program for the restoration of movements in neurologically impaired patients by functional electrical stimulation.

Acknowledgements. This work was supported by a fellowship grant from the Spinal Cord Research Foundation of Paralyzed Veterans of America (No. 923), a grant from the Pittsburgh Supercomputing Center (No. BCS900007P), and the NIH–NINDS neural prosthesis program (NO1-NS-9-2356).

Appendix. Muscle torque-angle relationship

In this appendix, the torque-angle relationship of muscle is discussed in relation to the equilibrium point control. In (2), muscle torque is linearly related to its stiffness. This relation implies a nonlinear torque-angle relation.

To see this clearly, let us take the flexor as an example, whose torque-stiffness relation is given by:

$$T_f = m_f K_f + b_f \tag{A.1}$$

Since

$$K_f = \frac{dT_f}{d\theta}$$

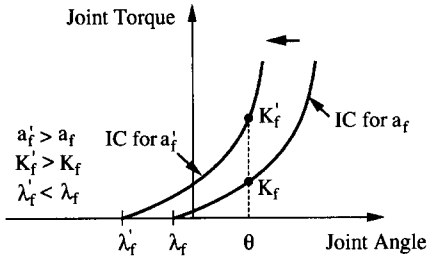

Fig. 8. An increase in muscle activation shifts the invariant characteristic (IC) curve towards the left. At a given joint position, θ, an IC curve is associated with an activation level, a_f, which in turn determines a stiffness, K_f, for the joint angle. When muscle activation is increased to a_f', the stiffness is correspondingly increased to K_f'. Since the joint angle, θ, remains the same, the IC curve must be shifted to the left by an amount of $\lambda_f - \lambda_f' = m_f \ln(a_f'/a_f)$. Thus, a decrease in muscle activation will cause the IC curve to shift towards the right on the angle axis.

then we have the differential equation of the following:

$$T_f = m_f \frac{dT_f}{d\theta} + b_f \tag{A.2}$$

Rearranging and integrating (A.2), one obtains the result,

$$\frac{\theta - \lambda_f}{m_f} = \ln(T_f - b_f) \quad \theta \geqslant \lambda_f$$

in which λ_f is the integration constant. This relation may be expressed in a more familiar way:

$$T_f = \exp\left(\frac{\theta - \lambda_f}{m_f}\right) + b_f \quad \theta \geqslant \lambda_f \tag{A.3}$$

Equation (A.3) gives the explicit exponential torque-angle relationship. It defines a family of torque-angle curves with respect to parameter λ_f, which represent the torque-angle relation only for the angles $\theta \geqslant \lambda_f$. Equation (A.3) is an approximation of muscle invariant characteristics (IC) as suggested by Feldman (1986).

The muscle stiffness is also dependent on the joint angle since:

$$K_f = \frac{dT_f}{d\theta} = \frac{1}{m_f} \exp\left(\frac{\theta - \lambda_f}{m_f}\right) \tag{A.4}$$

From (A.4), we can further see that the parameter λ_f is dependent on muscle activation. This is because the stiffness K_f is proportional to muscle activation a_f [see (3) in the text]. Under static conditions, when muscle activation changes, the joint angle θ will not change. Thus, λ_f must change to satisfy (A.4). The effect of changing λ_f is to shift the IC curve along the joint angle axis. For example, if muscle activation is varied to a_f' from a_f, then λ_f is shifted to λ_f' correspondingly. According to (3) and (A.4), we have,

$$\exp\left(\frac{\theta - \lambda_f'}{m_f}\right) = \left(\frac{a_f'}{a_f}\right) \exp\left(\frac{\theta - \lambda_f}{m_f}\right)$$

and the amount of shift is given by:

$$\lambda_f - \lambda_f' = m_f \ln(a_f'/a_f) \tag{A.5}$$

The equation clearly shows the dependence of λ_f' on muscle activation. If muscle activation is increased $(a_f' - a_f)$, then λ_f' is smaller than λ_f, which means that the muscle IC curve is shifted towards the left, as shown in Fig. 8. Similarly, a decrease in muscle activation will cause the IC curve to shift towards the right.

References

Atkeson CG, Hollarbach JM (1985) Kinematic features of unrestrained vertical arm movements. J Neurosci 5:2318–2330

Bennett DJ, Hollarbach JM, Xu Y, Hunter IW (1992) Time-varying stiffness of human elbow joint during cyclic voluntary movements. Exp Brain Res 88:433–442

Bizzi E, Dev P, Morasso P, Polit A (1978) Effect of load disturbances during centrally initiated movements. J Neurophysiol 41:542–556

Bizzi E, Hogan N, Mussa-Ivaldi FA, Giszter S (1992) Does the nervous system use equilibrium-point control to guide single and multiple joint movements? Behav Brain Sci 15:603–613

Bryson, AE Jr, Ho YC (1975) Applied optimal control. Wiley, New York

Cannon SC, Zahalak GI (1982) The mechanical behavior of active human skeletal muscle in small oscillations. J Biomech 15:111–121

Carter RR, Crago PE, Gorman PH (1993) Nonlinear stretch reflex interaction during cocontraction. J Neurophysiol 69:943–952

Feldman AG (1986) Once more on the equilibrium-point hypothesis (λ-model) for motor control. J Motor Behav 18:17–54

Feldman AG, Orlovsky GN (1972), The influence of different descending systems on the tonic stretch reflex in the cat. Exp Neurol 37:481–494

Feldman AG, Adamovich SV, Ostry DJ, Flanagan JR (1990) The origin of electro-myograms – explanation based on the equilibrium point hypothesis, IN Winters J, Woo S (eds) Multiple muscle systems, biomechanics and movement organization. Springer, Berlin Heidelberg New york

Flanders M, Herrmann U (1992) Two components of muscle activation: scaling with the speed of arm movement. J Neurophysiol 67: 931–943

Flash T (1987) The control of hand equilibrium trajectories in multi-joint arm movements. Biol Cybern 57:257–274

Gottlieb GL, Agarwal GC (1971) Effects of initial conditions on the Hoffman reflex. J Neurol Neurosur Psychiatry 34:226–230

Gottlieb GL, Corcos DM, Agarwal GC (1989), Strategies for the control of voluntary movements with one mechanical degree of freedom. Behav Brain Sci 12:189–210

Hasan Z (1986) Optimized movement trajectories and joint stiffness in unperturbed, inertially loaded movements. Biol Cybern 53: 373–382

Hoffer JA, Andreassen S (1981) Regulation of soleus muscle stiffness in premammillary cats: intrinsic and reflex components. J Neurophysiol 45:267–285

Hogan N (1984) An organizing principle for a class of voluntary movements. J Neurosci 4:2745–2754

Houk JC, Rymer WZ (1981) Neural control of muscle length and tension. In: Brooks VB (ed) Handbook of physiology sect 1, The nervous system vol II, part 1. American Physiological Society, Bekerda, Md, pp257–324

Humphrey DR, Reed DJ (1983) Separate cortical systems for control of joint movement and joint stiffness: reciprocal activation and co-activation of antagonist muscles. In: Desmedt JE (ed) Advances in neurology vol 39. Motor control mechanisms in health and disease. Raven, New York

Karst GM, Hasan Z (1987) Antagonist muscle activity during human forearm movements under varying kinematic and loading conditions. Exp Brain Res 67:391–401

Kearney RE, Hunter IW (1990) System identification of human joint dynamics. CRC Crit Rev Biomed Eng 18:55–87

Kirk DE (1970) Optimal control theory, an introduction. Prentice-Hall, Englewood Cliffs

Lacquaniti F, Licata F, Soechting JF (1982) The mechanical behavior of the human forearm in response to transient perturbations. Biol Cybern 44:35–46

Latash ML (1992) Virtual trajectories, joint stiffness, and changes in the limb natural frequency during single-joint oscillatory movements. Neuroscience 49:209–220

Latash ML, Gottlieb GL (1991) Reconstruction of shifting elbow joint compliant characteristics during fast and slow movements. Neuroscience 43:697–712

Lestienne F (1979) Effects of inertial load and velocity on the braking process of voluntary limb movements. Exp Brain Res 35:407–418

Marsden CD, Obeso JA, Rothwell JC (1983) The function of the antagonistic muscle during fast limb movements in man. J Physiol (Lond) 335:1–13

Matthews PBC (1986) Observations on the automatic compensation of reflex gain on varying the pre-existing level of motor discharge in man. J Physiol (Lond) 374:73–90

Mustard E, Lee RG (1987) Relationship between EMG patterns and kinematic properties for flexion movements at the human wrist. Exp Brain Res 66:247–256

Nagasaki H (1989) Asymmetric velocity and acceleration profiles of human arm movements. Exp Brain Res 74:319–326

Nichols TR (1987) The regulation of muscle stiffness, implications for the control of limb stiffness. In: Hebbelinck M, Shephard RJ (eds) Medicine and sport science, Vol 26. Karger, Basel, pp 36–47

Nichols TR, Houk JC (1976) Improvement in linearity and regulation of stiffness that results from actions of stretch reflex. J Neurophysiol 39:119–142

Nichols TR, Koffler-Smulevitz D (1991) Mechanical analysis of heterogenic inhibition between soleus muscle and the pretibial flexors in the cat. J Neurophysiol 66:1139–1155

Rack PMH, Westbury DR (1969) The effects of length and stimulus rate on tension in the isometric cat soleus muscle. J Physiol 204:443–460

Robinson SM (1972) A quadratically convergent algorithm for general nonlinear programming problems. Math Program 3:145–156

Soechting JF, Dufresne JR, Lacquaniti F (1981) Time-varying properties of myotatic response in man during some simple motor tasks. J Neurophysiol 46:1226–1243

Uno Y, Kawato M, Suzuki R (1989) Formation and control of optimal trajectory in human multijoint arm movement. Biol Cybern 61:89–101

Winters JM, Stark L (1987) Muscle models: what is gained and what is lost by varying model complexity. Biol Cybern 55:403–420

Wu CH, Houk JC, Young KY Miller LE (1990) Nonlinear damping of limb motion. In: Winters J Woos (eds), Multiple muscle systems, biomechanics and movement organization, chap 13. Springer, Berlin Heidelberg, New York